Full Paper

Numerical investigation of turbulent flow and heat transfer for enhancing performance of gas turbine blade with rib turbulators

Pilaisiri Chaisri and Theeradech Mookum*

School of Science, Mae Fah Luang University, Chiang Rai, Thailand

*Corresponding author, e-mail: theeradech@mfu.ac.th

Abstract: We numerically investigate the effects of rib turbulators on turbulent flow and heat transfer in a gas turbine blade with impingement cooling. The 45°-angled ribs are attached on two opposite walls of the blade with two ribbed channels. Three-dimensional steady-state Reynolds-averaged Navier-Stokes equations combined with the standard k-ε model and heat equation are used to analyse the turbulent flow, temperature distribution and cooling effectiveness. The numerical results indicate that a blade with ribs generates more re-circulation regions and secondary flows, leading to higher turbulent kinetic energy, wall shear stress and a 23.86% increase in cooling effectiveness. In addition, increasing inlet velocity increases the volume-averaged cooling effectiveness, volume-averaged turbulent kinetic energy and area-averaged wall shear stress.

Keywords: rib turbulators, turbulent flow and heat transfer, Reynolds-averaged Navier-Stokes equations, impingement cooling, cooling effectiveness

---

INTRODUCTION

Gas turbine technology is essential in various industrial applications, from power generation to aviation. In a gas turbine engine the high temperature generated from the combustion chamber, ranging between 1200-1500℃, can cause blade failure. Therefore, it is important to reduce the blade temperature and protect the blades from cracking. One key approach to enhancing gas turbine performance is to optimise the cooling techniques used for the turbine blades. Among many strategies, impingement cooling is considered a promising method for mitigating the damaging

effects of high-temperature operation. The rib turbulator has attracted considerable attention as an effective heat transfer enhancement for gas turbine blade impingement cooling [1, 2].

Several experimental studies have characterised internal cooling passages as rectangular channels with single or double passes. Techniques such as thermochromic liquid crystals, laser-Doppler velocimetry, liquid crystal thermography, particle image velocimetry and infrared thermography have been instrumental in quantifying heat transfer coefficients. In their work Cavallero and Tanda [3] employed thermochromic liquid crystals to measure local heat transfer in ribbed single-pass channels, uncovering notably higher average heat transfer coefficients compared to unribbed channels. Satta et al. [4] investigated flow and heat transfer in a rectangular channel featuring parallel 45°-angled ribs positioned on one or two opposing walls. The flow field was captured using laser-Doppler velocimetry while local heat transfer coefficients were measured through liquid crystal thermography. Liou et al. [5] used particle image velocimetry and infrared thermography techniques to study secondary flows and heat transfer within a two-pass ribbed parallelogram channel. Their findings revealed the presence of small counter-rotating swirls and an enhanced thermal performance compared to smooth-wall channels. Yang et al. [6] used infrared thermography to examine heat transfer and pressure loss in single-pass rectangular ribbed channels, demonstrating an increase in heat transfer coefficients with rising Reynolds numbers.

The focus of this study is the integration of 45°-angled ribs into blade geometry. These ribs are attached to two opposing walls, thus forming ribbed channels. This design is intended to cause controlled turbulence and alter flow patterns, which will influence heat transfer characteristics. The ribbed channel configuration is fundamentally different from conventional smooth-walled arrangements. According to previous studies, using this configuration resulted in a more pronounced deviation in flow behaviour and heat transfer characteristics. Liu et al. [7] examined heat transfer characteristics in single-pass rectangular channels with 45°- and 60°-angled rib turbulators and observed higher average Nusselt numbers for channels with 45°-angled ribs compared to those with 60°-angled ribs and smooth channels. Dhanasekaran and Wang [8] noted that in channels with 45°-angled ribs, the Nusselt number increases with rising Reynolds numbers and surpasses that in channels with smooth surfaces. Additionally, Ravi et al. [9] found that V-shaped ribs provide the highest level of heat transfer enhancement among 45°-angled, V, W and M rib configurations in their numerical study. Furthermore, Liou et al. [10] confirmed that 45°-angled ribs yield the highest heat transfer enhancement, followed by 135°- and 90°-angled ribs, surpassing that of a smooth surface.

The numerical simulations in this study rely on the application of three-dimensional steady-state Reynolds-averaged Navier-Stokes (RANS) equations, a well-established computational fluid dynamics technique [11]. The utilisation of RANS equations allows for accurate representation of the flow field within the blade, accounting for turbulence effects. Complementing this, the widely adopted standard k-ε turbulence model is employed to capture the complex interaction between turbulence and heat transfer. The heat equation, a fundamental component in thermal analysis, is integrated to illustrate temperature distributions within the blade. A comprehensive understanding of turbulent flow, temperature distribution and cooling effectiveness is obtained through this approach. Du et al. [12] used RANS equations to explore the influence of jet nozzle geometry on flow patterns and heat transfer performance. Fan et al. [13] employed RANS equations and the standard k-ω model to investigate the effects of film hole geometry and mass flow on vortex cooling for the leading edge of a gas turbine blade.

Due to the complexity of the turbine blade, some researchers have chosen to focus on specific components. Previous numerical studies focused primarily on the leading edge. These studies employed the computational fluid dynamics simulations along with numerical models and turbulence equations to analyse flow patterns and heat transfer characteristics. The studies explored innovative cooling designs and configurations such as impingement cooling, film cooling, swirl cooling and combined techniques. Lin et al. [14] conducted an innovative leading-edge impingement cooling design featuring double swirl chambers that achieve 24% higher heat transfer enhancement than impingement cooling with inline multiple jets. Zhou et al. [15] examined the effects of film cooling hole locations on flow patterns and heat transfer in a combined impingement and effusion cooling setup at the leading edge of a turbine blade. They concluded that the impingement/effusion cooling case with a 0° inclined angle and staggered arrangement between film cooling holes and jet holes exhibits the most effective cooling performance. Mousavi et al. [16] simulated flow in swirl chambers and double swirl chambers and found that with constant geometrical parameters, enhancing heat transfer by up to 27% is achievable simply by employing a better inlet configuration at each section. Wu et al. [17] investigated four different composite cooling configurations combining swirl cooling and impingement cooling. Fan [18] introduced a novel vortex double-wall cooling system for gas turbine blades' leading-edges. The results indicated that vortex double-wall cooling surpasses impingement double wall cooling by 9.7% in terms of thermal performance.

Previous studies have focused on rib-turbulated cooling configurations with square or rectangular channels and single-pass or two-pass layouts, along with impingement cooling within the leading-edge passage. In this study we design a complete gas turbine blade incorporating two ribbed channels and a leading-edge passage. Within the ribbed configuration, 45°-angled ribs are attached to opposing walls, aligned with the main flow direction. Through numerical simulations, we aim to analyse the effects of rib turbulators on flow patterns, temperature distribution and local cooling effectiveness. Additionally, we examine the effects of coolant inlet velocity on these parameters.

COMPUTATIONAL METHODOLOGY

The blade geometry features three-dimensional shapes with rib turbulator. The 3D computer-aided design incorporates cooling methods for enhancing cooling effectiveness through sophisticated engineering.

Computational Domains

The computational domains represent three-dimension blade geometry with rib and without rib turbulator for internal cooling with no trailing edge effect. The computational domain for the blade with two channels and a 45°-angled ribbed wall, configured with tip holes is shown in Figure 1. The first channel connects to the leading passage via 5 impinging holes of 0.001 m in diameter. The second channel has three passages with two bends and two inlets of 0.0231 m in diameter (Figure 1b). Each channel has ribs on two opposite walls. The rib height is 0.0014 m and the pitch length is 0.011 m. The tip cap has 9 holes with a diameter of 0.003 m (Figure 1a). The blade has a thickness of 0.0015 m, a length of 0.09189 m, a width of 0.04516 m and a height of 0.12331 m (Figures 1a,c).
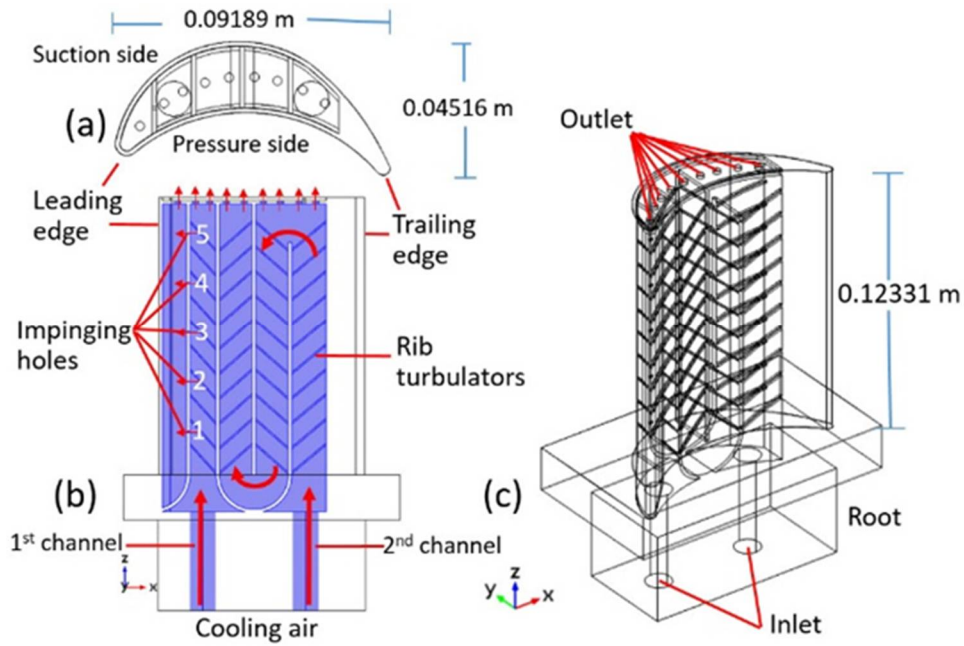
Figure 1. Geometry of blade with rib turbulators: top view (a), front view (b), 3D view (c)

Governing Equations

The velocity and temperature of the air inside the blade were simulated, taking into account the injection of cooling air through inlet nozzles and its exit through outlet holes (Figure 1c). The governing equations for this analysis were derived from transport phenomena. Specifically, the velocity and temperature of the air (fluid) are described by steady-state RANS equations while the temperature distribution within the blade (solid) is determined by the steady-state heat conduction equation. In fluid mechanics an essential application of transport analysis is to determine the velocity profile of a fluid flow. Within the fluid region (air), the steady-state RANS equations, based on Boussinesq hypothesis for compressible fluid flow and heat transfer, can be expressed as [19]:

$$\frac{\partial}{\partial x_i}(\rho_{air} u_i) = 0, \tag{1}$$

$$\frac{\partial}{\partial x_j}(\rho_{air} u_i u_j) = -\frac{\partial p}{\partial x_i} + \frac{\partial}{\partial x_j}\left[(\mu_{air} + \mu_t)\left(\frac{\partial u_i}{\partial x_j} + \frac{\partial u_j}{\partial x_i}\right) - \frac{2}{3}(\mu_{air} + \mu_t)\frac{\partial u_i}{\partial x_i} - \frac{2}{3}\rho_{air}k\right], \tag{2}$$

$$\frac{\partial}{\partial x_i}(\rho_{air} C_{p,air} u_i T) = \frac{\partial}{\partial x_i}\left[(\lambda_{air} + \lambda_t)\frac{\partial T}{\partial x_i}\right], \tag{3}$$

where i and j are tensor notations, u is the velocity, p is the pressure, T is the temperature, ρ_{air} is the density of air, μ_{air} is the viscosity of air, $C_{p,air}$ is the heat capacity of air, and λ_{air} is the thermal conductivity of air. The eddy viscosity μ_t and conductivity λ_t are calculated as $\mu_t = \rho_{air}C_\mu k^2/\varepsilon$ and $\lambda_t = C_{p,air}\mu_t/Pr_t$ respectively, where Pr_t is the turbulent Prandtl number set to 0.85 [20].

The standard $k-\varepsilon$ turbulence model is widely employed in computational fluid dynamics. This model relies on the concept of eddy viscosity. It involves solving two partial differential equations, known as transport equations, which are used to determine the turbulent kinetic energy (k) and the turbulence eddy dissipation (ε). The steady-state $k-\varepsilon$ turbulence model is as follows:

$$\frac{\partial}{\partial x_i}(\rho_{air}ku_i) = \frac{\partial}{\partial x_i}\left[\left(\mu_{air} + \frac{\mu_t}{\sigma_k}\right)\frac{\partial k}{\partial x_i}\right] + G_k - \rho_{air}\varepsilon, \tag{4}$$

$$\frac{\partial}{\partial x_i}(\rho_{air}\varepsilon u_i) = \frac{\partial}{\partial x_i}\left[\left(\mu_{air} + \frac{\mu_t}{\sigma_\varepsilon}\right)\frac{\partial \varepsilon}{\partial x_i}\right] + \frac{C_1\varepsilon}{k}G_k - C_2\rho_{air}\frac{\varepsilon^2}{k}, \tag{5}$$

where

$$G_k = \mu_t\left[\frac{\partial u_i}{\partial x_j}\left(\frac{\partial u_i}{\partial x_j} + \frac{\partial u_j}{\partial x_i}\right) - \frac{2}{3}\left(\frac{\partial u_i}{\partial x_i}\right)^2\right] - \frac{2}{3}\rho_{air}k\frac{\partial u_i}{\partial x_i}. \tag{6}$$

The constants have the following values [21]: $C_1 = 1.44$, $C_2 = 1.92$, $C_\mu = 0.09$, $\sigma_k = 1.0$ and $\sigma_\varepsilon = 1.3$.

In the solid region (blade), the steady-state heat conduction equation is given by

$$\frac{\partial}{\partial x_i}\left[\lambda_s\frac{\partial T}{\partial x_i}\right] = 0, \tag{7}$$

where λ_s is the thermal conductivity of the solid.

Boundary Conditions

To solve the set of equations (1)-(7), the boundary conditions are specified as follows. On the inlet the cooling air is injected into the blade with inlet velocity U_{in}, cooling temperature T_c, inlet turbulent kinetic energy k_{in}, and inlet turbulent dissipation rate ε_{in}. On the outlet the total stress and the gradient of turbulent kinetic energy and turbulent dissipation rate are set to zero. The gradient of temperature is set to zero at the outlet and the root wall. The heat flux boundary condition is set at the blade surface as

$$q = h(T_\infty - T), \tag{8}$$

where h is the heat transfer coefficient and T_∞ is the mainstream temperature. The boundary condition near the inner wall is given by the wall function [22]. The wall heat flux can be expressed as

$$q_w = \frac{\rho_{air}C_{p,air}C_\mu^{1/4}k^{1/2}(T_w - T)}{T^+}, \tag{9}$$

where T_w is the wall temperature and T^+ is the dimensionless temperature. The gradient of turbulent kinetic energy is zero and the kinetic dissipation rate is

$$\varepsilon = \frac{\rho_{air}C_\mu k^2}{\kappa\delta_w^+\mu_{air}}, \tag{10}$$

where κ is the Karman constant equal to 0.41. The distance δ_w^+ is defined as

$$\delta_w^+ = \frac{\delta_w\rho_{air}C_\mu^{1/4}k^{1/2}}{\mu_{air}}, \tag{11}$$

where δ_w is a small distance between the fluid and the wall.

Mesh Generation

The quality of mesh elements is a dimensionless quality between 0 to 1, where 1 is the highest quality and 0 indicates a degenerated element. The total number of tetrahedral elements for the blade with ribs is 938061 and for the blade without ribs is 938003. The average element qualities are 0.6848 and 0.6707 respectively, which is good enough to conduct accurate calculations (Figure 2).
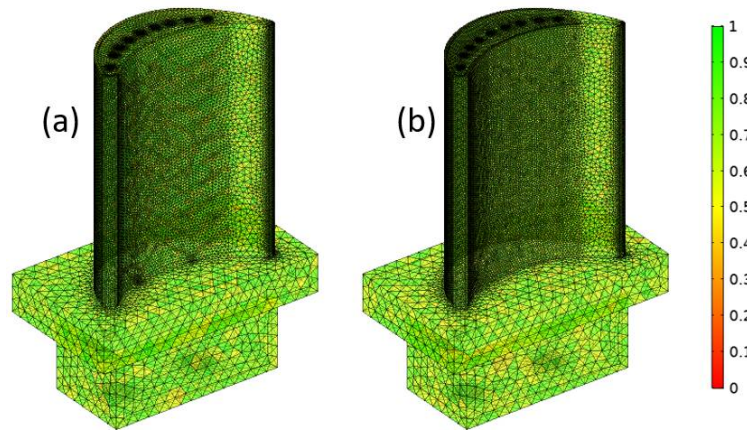
Figure 2. Computational meshes for blades as elements with ribs (a) and without ribs (b)

RESULTS AND DISCUSSION

In this study two types of blades were considered: blades with and without ribs. For the numerical investigation, the physical properties of the air and blade material (Inconel 718) in COMSOL Multiphysics software, dependent on the temperature, are presented in Table 1. The heat transfer coefficient h of a nickel-based superalloy was calculated by Fu et al. [23]. The cooling temperature $T_c = 400°C$, the mainstream temperature $T_\infty = 1200°C$, the inlet turbulent kinetic energy $k_{in} = 0.005 \ m^2/s^2$, and the inlet turbulent dissipation rate $\varepsilon_{in} = 0.0054786 \ m^2/s^3$. The coupled six partial differential equations (1)-(7), which are subjected to the boundary conditions, were solved with COMSOL Multiphysics software based on the finite element method.

**Table 1.** Temperature-dependent material properties

Parameter	Value	Unit
$\boldsymbol{\rho_{air}}$	$352.7T^{-1}$	$\boldsymbol{kg/m^3}$
$\boldsymbol{\mu_{air}}$	$3.893\times10^{-6} +5.754\times10^{-8}T -2.676\times10^{-11}T^2 +9.710\times10^{-15}T^3 -1.356\times10^{-18}T^4$	$\boldsymbol{kg/(m.s)}$
$\boldsymbol{C_{p,air}}$	$1093 -0.6356T +1.634\times10^{-3}T^2 -1.413\times10^{-6}T^3 +5.595\times10^{-10}T^4 -8.663\times10^{-14}T^5$	$\boldsymbol{J/(kg.K)}$
$\boldsymbol{\lambda_{air}}$	$-8.404\times10^{-4} +1.107\times10^{-4}T -8.636\times10^{-8}T^2 +6.314\times10^{-11}T^3 -1.882\times10^{-14}T^4$	$\boldsymbol{W/(m.K)}$
$\boldsymbol{\lambda_s}$	$3.496 +0.02673T -1.118\times10^{-5}T^2 +3.607\times10^{-9}T^3 +8.236\times10^{-14}T^4$	$\boldsymbol{W/(m.K)}$
$\boldsymbol{h}$	$-219.581 +\exp\left(5.75 -3.7\times10^{-4}T +4.2\times10^{-7}T^2\right)$	$\boldsymbol{W/(m^2 \cdot K)}$

Note: ρ_{air} = density of air, μ_{air} = dynamic viscosity of air, $C_{p,air}$ = heat capacity of air, λ_{air} = thermal conductivity of air, λ_s = thermal conductivity of solid, h = heat transfer coefficient

Mesh Independence Study and Convergence Criteria

To conduct the mesh independence study, we investigated four different mesh systems: 109631; 212621; 473339; and 938061 tetrahedral elements for the blade with ribs, and 109829; 212749; 473626; and 938003 elements for the blade without ribs. The convergence criteria were set as residuals below 10^{-5} for continuity, momentum and turbulent equations, and at 10^{-8} for the energy equation. The number of nodes ranged from 504302 to 4315080. The temperature range was

between 400-1200℃, with averages of 880-891℃ and standard deviations of 195-215℃. The average temperatures of the blades were compared and the results are depicted in Figure 3. The relative errors are below 0.6% as the number of elements increase. Consequently, we utilised the finest meshes (938061 elements for the blade with ribs and 938003 elements for the blade without ribs) for all simulations in this study.
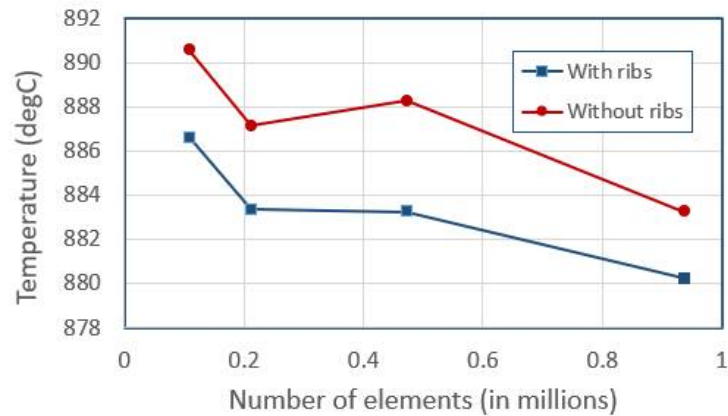
**Figure 3.** Average temperatures of blades for different mesh systems

Effects of Rib Turbulators

To investigate the effects of the rib turbulators, the cooling air was injected into the blade with a constant rate U_{in} = 70 m/s. Figure 4 illustrates the normalised velocity vector coloured by its magnitude (m/s) in the leading-edge passage and the first channel on cross section at the centre of impinging holes nos. 1, 3 and 5 (Figure 1). We observed that the flow coming from the inlet hits the ribs and generates more re-circulation regions in the blade with ribs. In the first channel (P1) of the blade with ribs (Figure 4a), a pair of counter-rotating vortexes is generated. Two vortices are initiated near the walls (no. 1) and gradually move away from the walls (no. 5). For the blade without ribs (Figure 4b), the flow is nearly laminar and there is no re-circulation region. In the leading-edge passage (P2), the jet flow from the impinging holes hits the wall directly and generates a larger vortex near the pressure side and a small one near the suction side. As the geometry in the leading-edge passage of both types is the same, the flow characteristics are not significantly different.
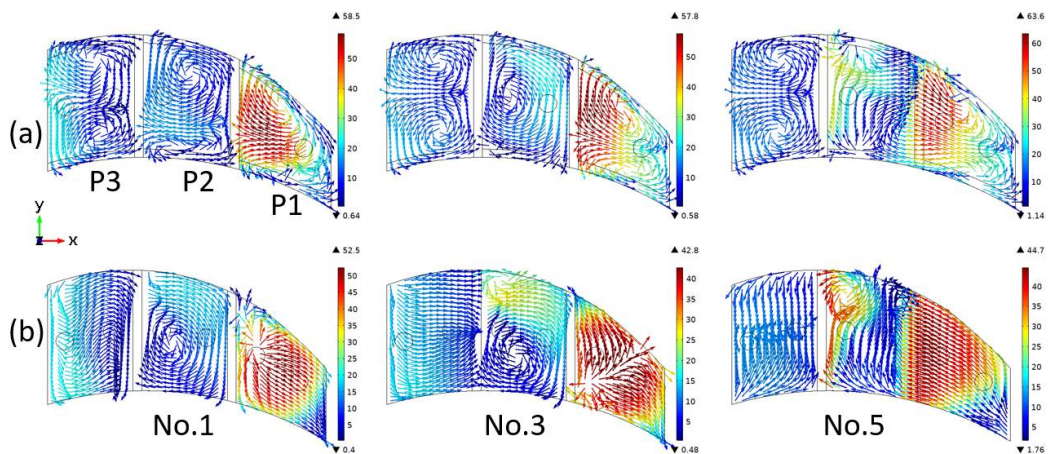
Figure 5 shows the normalised velocity vector coloured by its magnitude (m/s) in the second channel cross section at the centre of impinging holes nos.1, 3 and 5. For the cooling airflow for the blade with ribs, two pairs of counter-rotating vortices are generated in the passages P1, P2 and P3. The flow moves in the same direction towards the leading edge while in passage P2 it moves toward the trailing edge and generates a large vortex (Figure 5a). For the blade without ribs (Figure 5b), a small vortex is generated near the wall in passage P2.

Figure 6 illustrates the velocity magnitude near the internal wall surfaces for both the blade with and without ribs. The blade with ribs has stronger flow near the inlet and weaker flow in the second and third passages of the second channel. However, near the tip holes and the bend-shaped region, the flow strengthens again. The blade without ribs exhibits strong flow along the first passages of both channels and weaker flow in the second and third passages of the second channel.At the leading-edge passage, the suction side wall is directly hit by the jet flow from the impinging holes, resulting in strong flow on the target surface. The presence of ribs suppresses the velocity of the cooling airflow.
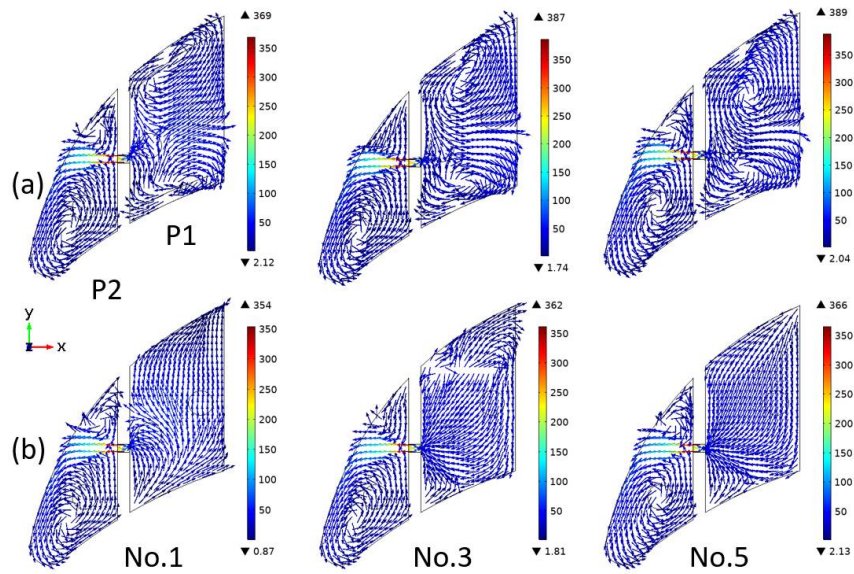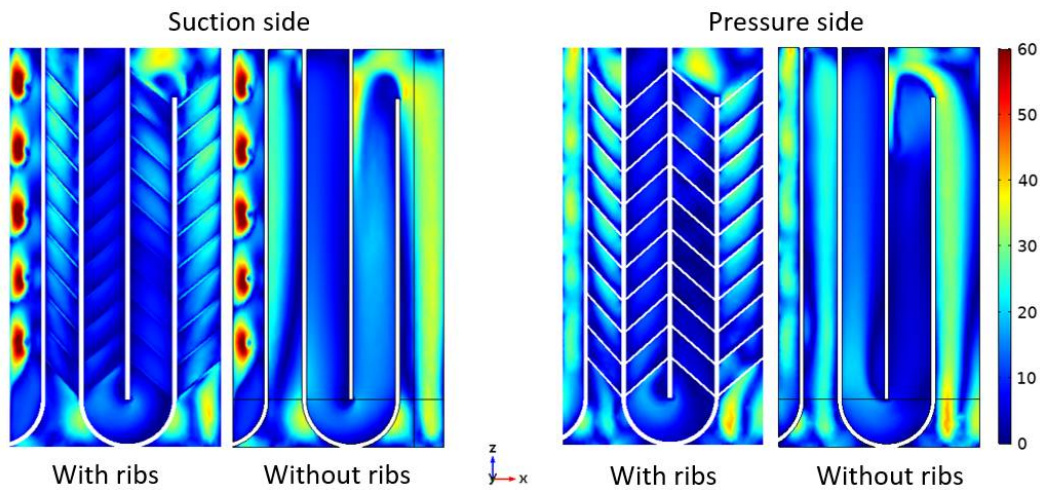
Figure 4. Normalised velocity vector (m/s) in leading-edge passage and first channel of blades with ribs (a) and without ribs (b)


Figure 5. Normalised velocity vector (m/s) in second channel of blades with ribs (a) and without ribs (b)

Figure 6. Velocity magnitude (m/s) near inner wall of blades

According to Gao et al. [24], the formation of secondary flow in two-pass ribbed channels is caused by ribs, main flow, bends and corners. As shown in Figure 7, the inner wall's secondary flow is generated by the presence of ribs, bends and impinging holes on the blade. In the blade with ribs, vortices near the inlet are formed by the first rib and outer U-bend in both channels, and the rib-induced flow moves between ribs towards the main flow direction, being stronger in the first channel and weaker in the second and third. Interaction between the first bend and rib forms a vortex, while that between the second bend and rib creates secondary flow due to centrifugal force. In the blade without ribs secondary flow is generated via two bends and impinging holes, with two vortices near the inlet formed by the outer U-bend in both channels. The strong secondary flow in the leading passage is generated by high-velocity air jet impinging towards the target surface, which then expands along the wall.
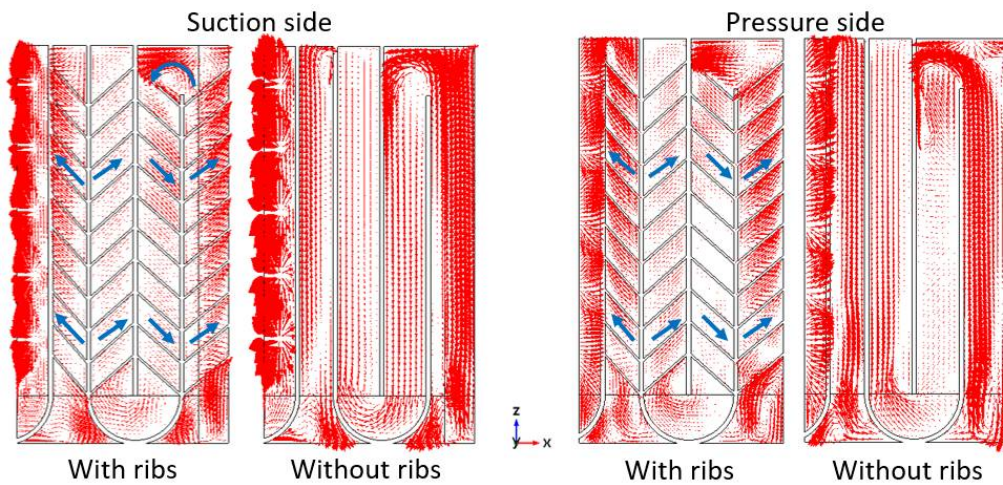
Figure 7. Secondary flow (m/s) near inner wall of blades

The turbulent kinetic energy represents the fluctuation of fluid velocity. It can affect the development of turbulent flow. Figure 8 depicts the distribution of turbulent kinetic energy near the inner wall surfaces of blades with and without ribs. The blade with ribs has a higher overall turbulent kinetic energy compared to the blade without ribs, which is evident at the leading-edge passage, first passage of the ribbed channels, and near the inlet in the smooth channel. The maximum level is found on the suction side at the leading-edge passage, where the jet flow from the impinging holes impacts the wall. The levels of turbulent kinetic energy are correlated with the complexity of the secondary flow as seen in Figure 7.

The wall shear stress (WSS) is defined by

$$\tau_w = (\mu_{air} + \mu_t)\dot{\gamma}, \tag{12}$$

where $\dot{\gamma}$ is the shear rate, calculated as

$$\dot{\gamma} = \sqrt{\frac{1}{2}(\nabla\boldsymbol{u} + (\nabla\boldsymbol{u})^T) : (\nabla\boldsymbol{u} + (\nabla\boldsymbol{u})^T)}. \tag{13}$$

The secondary flow results in increasing the WSS leading to heat transfer enhancement on the wall [25]. Figure 9 presents the WSS on the suction side and pressure side of the blades with and without ribs. The high levels of WSS appear at the leading-edge passage on the suction side. The blade with ribs has higher WSS than one without ribs on the ribbed surfaces.
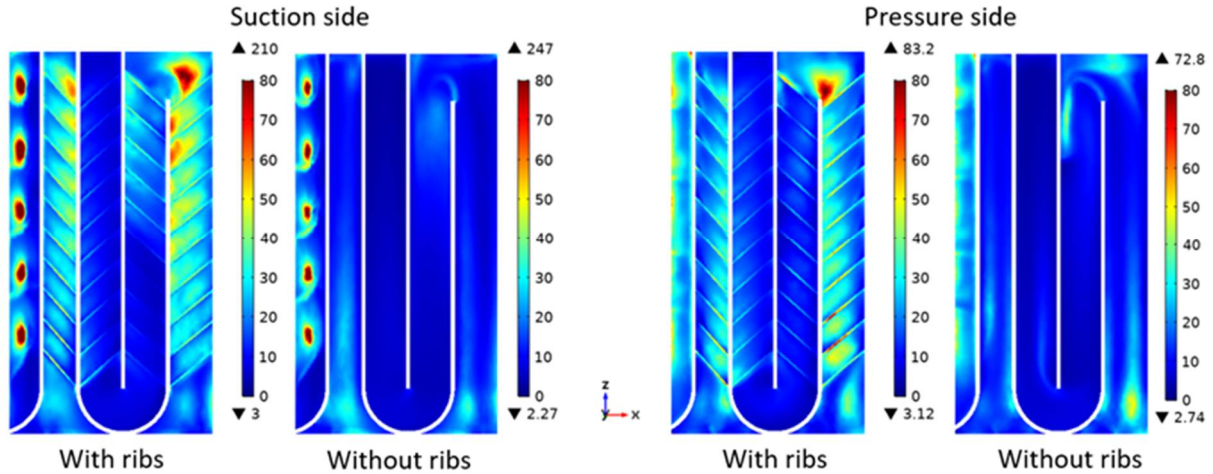
Figure 8. Turbulent kinetic energy (m²/s²) near inner wall of blades
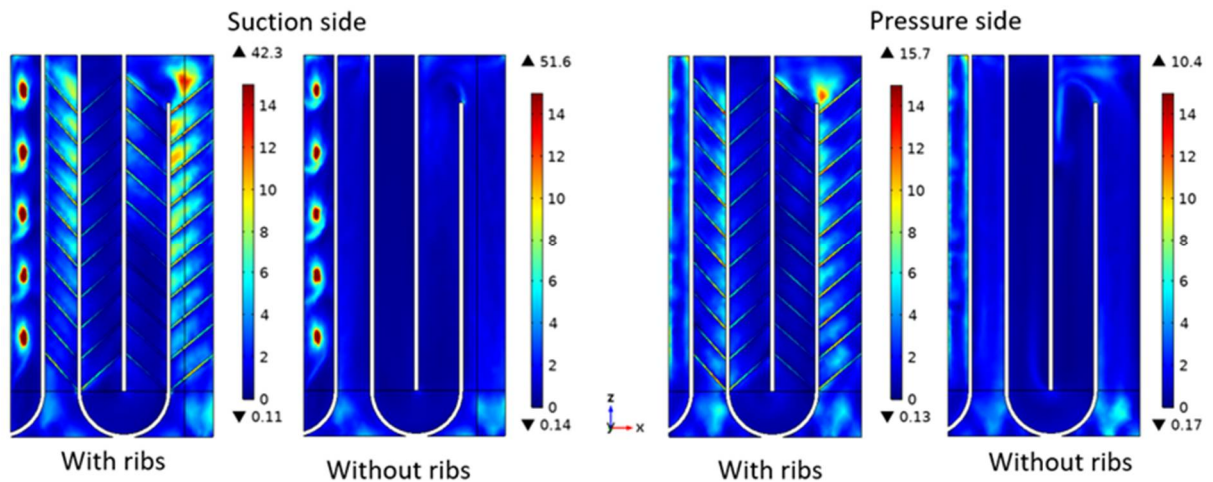
Figure 9. Wall shear stress (Pa) of blades

The local cooling effectiveness was calculated from the local temperature using the following equation:

$$\eta = \frac{T - T_\infty}{T_c - T_\infty}.$$ (14)

The volume-averaged and area-averaged cooling effectiveness are defined respectively as

$$\bar{\eta} = \frac{1}{V} \int_V \eta \, dV \ \text{ and } \ \bar{\eta}_A = \frac{1}{A} \int_A \eta \, dA,$$ (15)

where *V* and *A* represent volume of the solid region and area of the surface respectively.

The difference in cooling effectiveness near the inner wall on the suction and pressure sides of both types of the blade is depicted in Figure 10. Higher cooling effectiveness is obtained near the beginning of the inlet nozzle and weakens gradually with the distance to the end of the channels due to velocity factor. The cooling airflow entrapped by the ribs and circulating between the ribs leads to better cooling effectiveness in the blade with ribs.

The area-averaged cooling effectiveness ($\bar{\eta}_A$) decreases from the inlet to the outlet. In the first channel, $\bar{\eta}_A$ of the blade with ribs decreases by 41.46%, whereas for the blade without ribs it

decreases by 47.01%. In the second channel, the $\bar{\eta}_A$ decreases by 60.09% and 62.64% for the blade with and without ribs respectively.
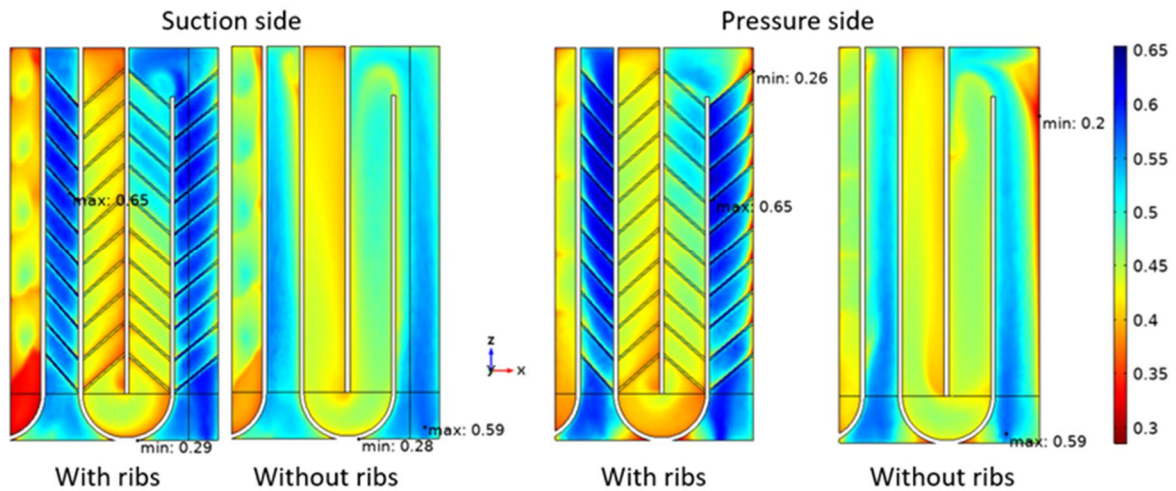
Figure 10. Cooling effectiveness near inner wall of blades

Figure 11 compares local cooling effectiveness of the blade bodies between blades with and without ribs. Results show higher cooling effectiveness in the blade with ribs, particularly at the first passage of each channel. Cooling air from the inlet passes through the first passage and heats up from the main stream temperature. Higher values of cooling effectiveness occur on channel walls, with lower values on trailing edges. The lowest values occur at top corners of the trailing edges, a critical area. Also, cooling effectiveness at the leading edge and third passage of the second channel is lower compared to that of the first channel. The values of volume-averaged cooling effectiveness of the blade bodies of blades with and without ribs are 0.33349 and 0.26925 respectively, which means that the rib turbulators can improve the cooling effectiveness by 23.86%.
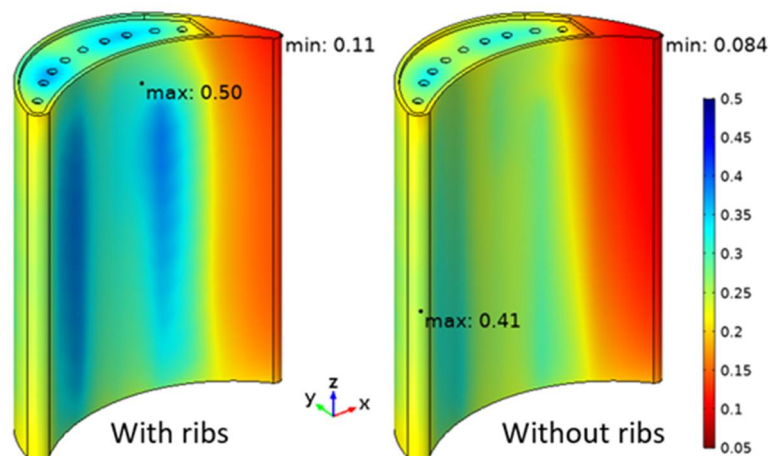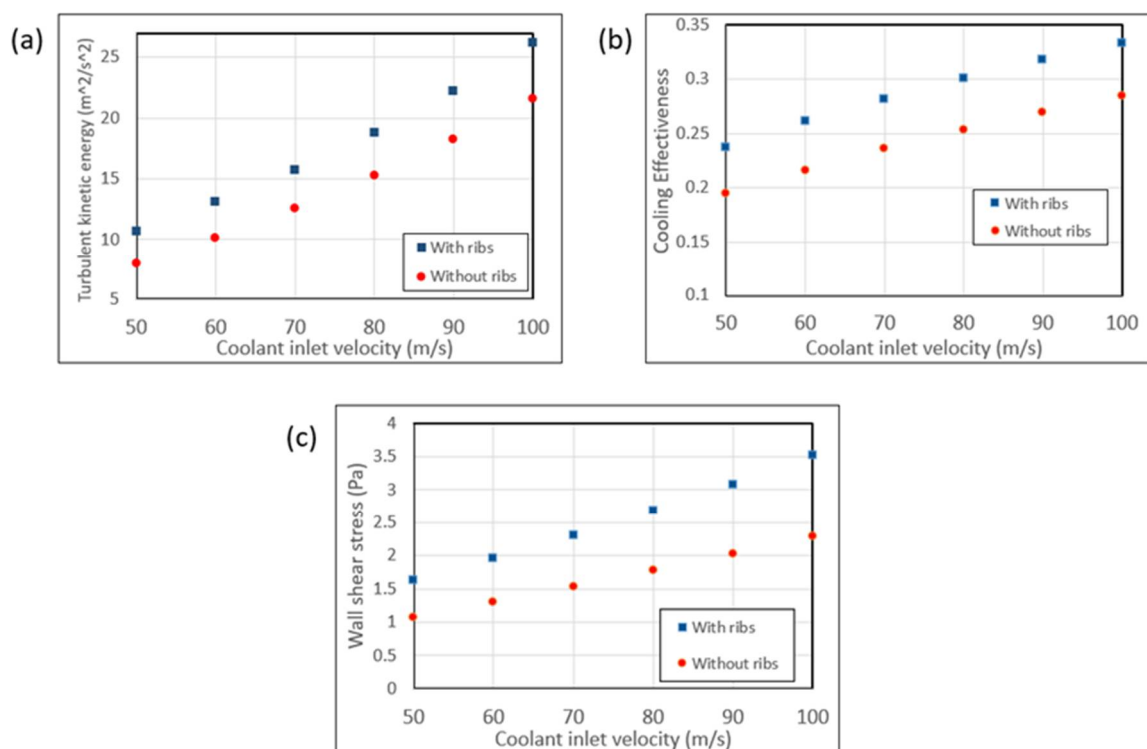

Figure 11. Cooling effectiveness of blades

Effects of Coolant Inlet Velocity

To analyse effects of coolant inlet velocity on turbulent kinetic energy, cooling effectiveness and WSS, six different cases of inlet velocity are investigated: 50, 60, 70, 80, 90 and 100 m/s corresponding to Reynolds numbers 50920, 61105, 71284, 81473, 91657 and 101841 respectively.

Figure 12 shows effects of inlet velocity on the volume-averaged turbulent kinetic energy, volume-averaged cooling effectiveness, and area-averaged WSS. With increasing inlet velocity, the turbulent kinetic energy, cooling effectiveness and WSS monotonically increase. However, for all ranges of inlet velocity, these values for the blade with ribs are larger than those for the blade without ribs. The trends is increase in turbulent kinetic energy and cooling effectiveness for both types of blades are quite similar, as shown in Figure 12a, b respectively. The WSS for the blade with ribs increases more rapidly than that for the blade without ribs, as shown in Figure 12c.

Figure 12. Effects of coolant inlet velocity on (a) volume-averaged turbulent kinetic energy (m^2/s^2), (b) volume-averaged cooling effectiveness, and (c) area-averaged WSS (Pa)

CONCLUSIONS

Turbulent flow and heat transfer in a gas turbine blade have been investigated using three-dimensional steady-state RANS equations, heat equation and standard k-ε model. Both rib-turbulated and impingement cooling techniques were used to improve heat transfer performance with a rib angle of 45° to the main flow direction being considered. The main conclusions of the study are

1. The blade with ribs generates more recirculation regions and secondary flows induced by its ribs, bends and impinging holes. Two vortices form near the inlet as a result of the first ribs and outer U-bend. The rib-induced secondary flow moves towards the main flow direction and a vortex

forms from the interaction between the first bend and rib. The strong secondary flows in the leading-edge passage are generated by the impinging holes.

2. The blade with ribs has higher overall turbulent kinetic energy than one without ribs, with high levels observed at the leading-edge passage and first ribbed channel. The highest level appears on the suction side at the leading-edge passage as a result of the jet flow from impinging holes hitting the wall. The complexity of secondary flows leads to increased WSS and higher levels of turbulent kinetic energy.

3. The blade with ribs has 23.86% higher volume-averaged cooling effectiveness compared to one without ribs, with higher effectiveness near the inlet nozzle and a gradual decrease along the channel distance due to velocity factor. The cooling airflow trapped by the ribs results in better cooling. The trailing edge has the lowest cooling effectiveness.

4. Increase in inlet velocity results in increase in volume-averaged turbulent kinetic energy, cooling effectiveness and WSS, with larger values for the blade with ribs. Both types of blade show similar trends in increase in turbulent kinetic energy and cooling effectiveness, but the ribbed blade's WSS increases faster.

ACKNOWLEDGEMENTS

REFERENCES

1. J. C. Han, "Recent studies in turbine blade cooling", *Int. J. Rotating Mach.*, **2004**, *10*, 443-457.
2. J. C. Han and H. C. Chen, "Turbine blade internal cooling passages with rib turbulators", *J. Propuls. Power*, **2006**, *22*, 226-248.
3. D. Cavallero and G. Tanda, "An experimental investigation of forced convection heat transfer in channels with rib turbulators by means of liquid crystal thermography", *Exp. Therm. Fluid Sci.*, **2002**, *26*, 115-121.
4. F. Satta, D. Simoni and G. Tanda, "Experimental investigation of flow and heat transfer in a rectangular channel with 45° angled ribs on one/two walls", *Exp. Therm. Fluid Sci.*, **2012**, *37*, 46-56.
5. T. M. Liou, S. W. Chang, C. Y. Huang, S. P. Chan and Y. A. Lan, "Particle image velocimetry and infrared thermography measurements in a two-pass 90-deg ribbed parallelogram channel", *Int. J. Heat Mass Transf.*, **2016**, *93*, 1175-1189.
6. W. Yang, S. Xue, Y. He and W. Li, "Experimental study on the heat transfer characteristics of high blockage ribs channel", *Exp. Therm. Fluid Sci.*, **2017**, *83*, 248-259.
7. J. Liu, J. Gao, T. Gao and X. Shi, "Heat transfer characteristics in steam-cooled rectangular channels with two opposite rib-roughened walls", *Appl. Therm. Eng.*, **2013**, *50*, 104-111.
8. T. S. Dhanasekaran and T. Wang, "Computational analysis of mist/air cooling in a two-pass rectangular rotating channel with 45-deg angled rib turbulators", *Int. J. Heat Mass Transf.*, **2013**, *61*, 554-564.
9. B. V. Ravi, P. Singh and S. V. Ekkad, "Numerical investigation of turbulent flow and heat transfer in two-pass ribbed channels", *Int. J. Therm. Sci.*, **2017**, *112*, 31-43.

10. T. M. Liou, S. W. Chang and S. P. Chan, "Effect of rib orientation on thermal and fluid-flow features in a two-pass parallelogram channel with abrupt entrance", *Int. J. Heat Mass Transf.*, **2018**, *116*, 152-165.

11. O. Reynolds, "On the dynamical theory of incompressible viscous fluids and the determination of the criterion", *Phil. Trans. Royal Soc. A*, **1895**, *186*, 123-164.

12. C. Du, L. Li, X. Wu and Z. Feng, "Effect of jet nozzle geometry on flow and heat transfer performance of vortex cooling for gas turbine blade leading edge", *Appl. Therm. Eng.*, **2016**, *93*, 1020-1032.

13. X. Fan, C. Du, L. Li and S. Li, "Numerical simulation on effects of film hole geometry and mass flow on vortex cooling behavior for gas turbine blade leading edge", *Appl. Therm. Eng.*, **2017**, *112*, 472-483.

14. G. Lin, K. Kusterer, A. H. Ayed, D. Bohn, T. Sugimoto, R. Tanaka and M. Kazari, "Numerical investigation on heat transfer in an advanced new leading edge impingement cooling configuration", *Propuls. Power Res.*, **2015**, *4*, 179-189.

15. J. Zhou, X. Wang, J. Li and Y. Li, "Effects of film cooling hole locations on flow and heat transfer characteristics of impingement/effusion cooling at turbine blade leading edge", *Int. J. Heat Mass Transf.*, **2018**, *126*, 192-205.

16. S. M. Mousavi, B. Ghadimi and F. Kowsary, "Numerical study on the effects of multiple inlet slot configurations on swirl cooling of a gas turbine blade leading edge", *Int. Commun. Heat Mass Transf.*, **2018**, *90*, 34-43.

17. F. Wu, L. Li, J. Wang, X. Fan and C. Du, "Numerical investigations on flow and heat transfer of swirl and impingement composite cooling structures of turbine blade leading edge", *Int. J. Heat Mass Transf.*, **2019**, *144*, Art.no.118625.

18. X. Fan, "Numerical research of a new vortex double wall cooling configuration for gas turbine blade leading edge", *Int. J. Heat Mass Transf.*, **2022**, *183*, Art.no.122048.

19. D. C. Wilcox, "Turbulence Modeling for CFD", 3rd Edn., Birmingham Press, San Diego, **2006**, pp.213-266.

20. W. M. Kays, "Turbulent prandtl number - Where are we?", *J. Heat Transf.*, **1994**, *116*, 284-295.

21. B. E. Launder and D. B. Spalding, "The numerical computation of turbulent flows", *Comput. Meth. Appl. Mech. Eng.*, **1974**. *3*, 269-289.

22. D. Lacasse, E. Turgeon and D. Pelletier, "On the judicious use of the k-ε model, wall functions and adaptivity", *Int. J. Therm. Sci.*, **2004**, *43*, 925-938.

23. P. Fu, P. Zhou, T.-Y. Zhao, Y.-P. Song and Z.-W. Huang, "Study of the heat transfer coefficient of a nickel-based superalloy in the end-quench test with air", *Int. J. Therm. Sci.*, **2020**, *155*, Art.no.106416.

24. T. Gao, J. Zeng, J. Zhu, J. Li and J. Gong, "Effects of rib angle and rib orientation on flow and heat transfer in two-pass ribbed channels", *J. Mech. Sci. Technol.*, **2018**, *32*, 513-526.

25. P. Singh, Y. Ji and S. V. Ekkad, "Experimental and numerical investigation of heat and fluid flow in a square duct featuring criss-cross rib patterns", *Appl. Therm. Eng.*, **2018**, *128*, 415-425.